Computer-AidedDesign

Taylor & Francis
Taylor & Francis Group

Truss-like structure design with local geometry control

Jikai Liu ⬤ and Yongsheng Ma ⬤

University of Alberta, Canada

ABSTRACT

This paper presents a local geometry control method when designing truss-like structures. Two kinds of local geometry measures are proposed: the local grid area and the local grid incircle radius. Both measures work effectively in constraining the local geometry and the selection is problem-dependent. To prove the effectiveness of the local geometry control, two shape optimization examples are studied by optimizing the nodal design freedoms. For topology optimization, the ground structure problem plus nodal design freedoms are employed and the simultaneous optimization approach is adopted to solve the optimization problem. It is highlighted that the local geometry constraints are dynamically applied to varying objects because of the grid merging caused by truss element elimination. The dynamic constraints would cause local fluctuation during the optimization process but would not impact the overall convergence.

1. Introduction

Truss or truss-like structure design has been actively investigated in the past three decades for its broad application scope. Different approaches have been developed such as the ground structure method, the density projection method [2], the evolutionary structural optimization (ESO) method [16], among which the ground structure method is definitely the most popular which can be tracked back to [9]. With this method, a dense grid is initially generated and the nodes are mutually connected to form the input ground structure. Cross-section area of each beam is applied as the design variable, and it could approach to zero value which means a topological change. A review about early developments of the ground structure method can be found in [4,5], and an educational Matlab program can be found in [21].

Even though intensively investigated, there are still drawbacks about the ground structure method that: the optimized solutions tend to employ complex topology; the result optimality is dependent on the initial guess and therefore extremely dense grid is generally required for the input ground structure. In addition, the optimized solution may be impractical because only selected sizes of the beams are available in reality.

In order to reduce the topology complexity, one possible approach is to remove the beams with sizes below a threshold value, and add the removed material back to the remaining beams. Given the negative impact, global optimality is lost and the optimal solution is strongly dependent on the threshold value [3]. Another approach is to penalize the intermediate beam sizes into either the lower or the upper bounds through the SIMP (Solid Isotropic Material with Penalization) method [6]. In this approach, the lower bound is assigned a small positive value to avoid singularity phenomenon and the upper bound is the full beam size. The penalization factor should be big enough to derive the pure binary solution.

To eliminate the dependence on the initial guess, exploration about adding nodes and beams during optimization [8,10,13,14] is conducted which has demonstrated good potential. However, a more popular solution is to allow additional design freedoms of moving nodes. As summarized by [1], two approaches: the alternative optimization and the simultaneous optimization, have been widely employed to involve the additional nodal freedoms.

For the alternative optimization, the simple implementation [17,18] is to alternately optimize the topological variables (beam cross-section size) with fixed shape variables (nodal positions) and shape variables with fixed topological variables. For instance, Wang et al. [17] applied the alternative optimization with fully stressed rule for the topology variables and the evolutionary node shift for the shape variables. Xia et al. [18] performed the gradient-based shape and topology optimization also following the alternative manner. With this approach, the

---

optimality criteria cannot be applied, but a local minimum is likely obtained even though it is not guaranteed [1]. Another implementation is to transform the original problem into a two-level nested problem [1,7,11], which is solved through the so called "implicit programming approach". However, only limited scale of design variables can be handled because of the non-smooth high-level problem.

A more direct approach is about the simultaneous optimization. This approach generally leads to a drastic increase of design variables, which may make the optimization algorithm quite complicated [17]. However, as commented by [1], the standard theory of nonlinear optimization applies and at least a local minimum can be found given certain scenarios [8]. Therefore, in this work, the authors apply the simultaneous optimization of the shape and topology variables.

More importantly, the main contribution is to realize the local geometry control. Specifically, two local geometry measures are proposed: the local grid area and the local grid incircle radius. With either measure, the local geometry constraint is applied by imposing an upper bound. Practically, it is meaningful of realizing the local geometry control in fulfillment of some functioning requirements, e.g. the sand protection of wire-wrapped screens and the permeability control of lattice structures. To the authors' knowledge, there is no similar research conducted before based on the literature survey.

It is also worth noticing that, scale control is also an important issue for truss-like structure design [19,20]. For small scale truss structures, the inverse homogenization is necessary for the optimization activity, while it is out of this paper's scope. Only the meso/macro truss structures will be studied in this paper.

The rest of this paper is organized as follows. Section 2 presents the simultaneous optimization problem and its solution. Section 3 introduces the two local geometry measures and the related local geometry control methods. A few shape and topology optimization examples are studied in Section 3, and the conclusion is given in Section 4.

2. The simultaneous optimization

2.1. Optimization problem

The popular compliance-minimization problem is employed to demonstrate the simultaneous optimization with local geometry control. The optimization problem is formulated as:

$$min. \quad \boldsymbol{F}^{\mathrm{T}}\boldsymbol{U}$$

$$s.t. \quad \boldsymbol{KU} = \boldsymbol{F}$$

$$\sum_{e=1}^{n} \rho_e v_e < v_{max} \quad or \quad \sum_{e=1}^{n} \rho_e < v_{max}$$

$$0 < \rho_{min} < \rho_e < 1 \tag{2.1}$$

where $\boldsymbol{K}$ is the assembled global stiffness tensor, $\boldsymbol{U}$ is the global displacement vector, and $\boldsymbol{F}$ is the global force vector. v_e is the volume of truss element e and v_{max} is the maximally allowed volume of the truss structure or the maximally allowed number of truss elements. The density based method [6] is applied for topology evolvement and so, the topological variable ρ_e is added to each truss element which varies within $[\rho_{min},1]$, where ρ_{min} is a small positive number to avoid the singularity phenomenon.

It is noted that:

$$\boldsymbol{K}_e = \boldsymbol{T}_e^T \rho_e^p \bar{\boldsymbol{K}}_e \boldsymbol{T}_e \tag{2.2}$$

where $\boldsymbol{T}_e$ is the coordinate transformation tensor [12]; $\overline{\boldsymbol{K}}_e$ is the stiffness tensor of truss element e in local coordinate system with the full cross-section value, while $\boldsymbol{K}_e$ is the stiffness tensor of truss element e in global coordinate system with interpolated cross-section value by ρ_e; and p (≥ 3) is the penalization factor to prevent intermediate densities. Assembly of $\boldsymbol{K}_e$ forms the global stiffness tensor $\boldsymbol{K}$.

On the other hand, truss elements in practice are often selected among a few discrete cross-section options. In that situation, some advanced multi-material interpolations should be applied. For instance, DMO (Discrete Optimization Optimization) [15] is a good multi-material interpolation scheme as presented in Eq. (2.3):

$$\boldsymbol{K}_e = \boldsymbol{T}_e^T \left\{ (\rho_{e1})^p [1 - (\rho_{e2})^p] \bar{\boldsymbol{K}}_{e1} \right.$$
$$\left. + (\rho_{e2})^p [1 - (\rho_{e1})^p] \bar{\boldsymbol{K}}_{e2} \right\} \boldsymbol{T}_e \tag{2.3}$$

in which $\bar{\boldsymbol{K}}_{e1}$ and $\bar{\boldsymbol{K}}_{e2}$ are stiffness tensors of truss element e in local coordinate system with the cross-section option 1 and 2, respectively; ρ_{e1} and ρ_{e2} are the densities related to cross-section option 1 and 2, respectively. The advantage of this multi-material interpolation scheme is that it will finally converge into either ($\rho_{e1} = 1, \rho_{e2} = 0$) or ($\rho_{e1} = 0, \rho_{e2} = 1$), which means a clearly identified cross-section option. This advanced scheme will be investigated in our future work.

2.2. Problem solution

To solve this shape optimization problem, the Lagrangian is constructed as:

$$L = \boldsymbol{F}^T \boldsymbol{U} - \tilde{\boldsymbol{U}}(\boldsymbol{KU} - \boldsymbol{F}) \tag{2.4}$$

in which $\tilde{\boldsymbol{U}}$ is the adjoint displacement field.

Correspondingly, the sensitivity analysis result on the nodal coordinate is:

$$\frac{\partial L}{\partial x_i} = -\sum_{e=1}^{n} U_e^T \frac{\partial K_e}{\partial x_i} U_e$$

$$= -\sum_{e=1}^{n} U_e^T \left(\frac{\partial T_e^T}{\partial x_i} \rho_e^p \bar{K}_e T_e + T_e^T \rho_e^p \frac{\partial \bar{K}_e}{\partial x_i} T_e \right.$$

$$\left. + T_e^T \rho_e^p \bar{K}_e \frac{\partial T_e}{\partial x_i} \right) U_e \qquad (2.5)$$

where U_e is the displacement vector of truss element e and x_i is the ith nodal coordinate.

Then, the sensitivity analysis result on the truss element density ρ_e is:

$$\frac{\partial L}{\partial \rho_e} = -\sum_{e=1}^{n} U_e^T \frac{\partial K_e}{\partial \rho_e} U_e \qquad (2.6)$$

Changes of the nodal positions and truss element densities can be determined through Eq. (2.7) and (2.8), which ensures that the Lagrangian changes in the steepest descent direction.

$$\frac{\partial x_i}{\partial t} = \sum_{e=1}^{n} U_e^T \frac{\partial K_e}{\partial x_i} U_e \qquad (2.7)$$

$$\frac{\partial \rho_e}{\partial t} = \sum_{e=1}^{n} U_e^T \frac{\partial K_e}{\partial \rho_e} U_e \qquad (2.8)$$

Design update of the shape variable and the topological variable is performed through Eq. (2.9) and (2.10), respectively

$$x_i^{k+1} = x_i^k + t \frac{\partial x_i}{\partial t} \qquad (2.9)$$

$$\rho_e^{k+1} = \rho_e^k + t \frac{\partial \rho_e}{\partial t} \qquad (2.10)$$

in which, t is the step length and k represents the iteration number.

It is noted that the inequality constraints are not necessary for shape optimization, because the design domain is bounded and the nodes can only move within it. On the other hand, the inequality constraints are mandatory for topology optimization; otherwise, no topological change would happen because all truss element densities approaching to 1 would provide the optimal structural compliance. In this work, the augmented Lagrange multiplier method is adopted to address the inequality constraints [18].

2.3. Optimization procedure

Procedure of the simultaneous optimization is listed below:

Step 1: Generate the input ground structure and prepare all the optimization related parameters.
Step 2: Perform the finite element analysis to compute the displacement vector U.
Step 3: Calculate the sensitivity information $\frac{\partial L}{\partial x_i}$ and $\frac{\partial L}{\partial \rho_e}$.
Step 4: Simultaneously update the shape variable x_i and the topological variable ρ_e.
Step 5: Check if the termination condition is satisfied. If no, repeat the step 2–4.

3. local geometry control

3.1. The local grid area

In [18], geometry control was realized to prevent truss elements from intersection. As shown in Fig. 1, if the vertex *v3* flips over the edge *v1-v2*, the truss elements intersect which is unreasonable in practice.
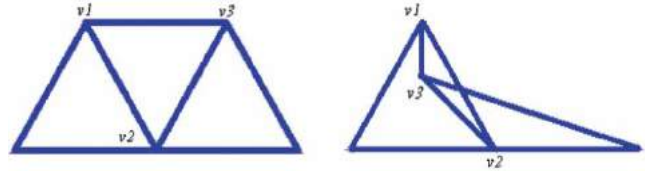

Figure 1. Example of truss element intersection: (a) Structure before truss element intersection, (b) Structure after truss element intersection.

Therefore, a non-intersection constraint was developed, as:

$$S_j \geq \underline{S} \quad j = 1, \dots, m$$

$$S_j = 0.5 * \det \begin{bmatrix} 1 & 1 & 1 \\ x_1 & x_2 & x_3 \\ y_1 & y_2 & y_3 \end{bmatrix} \qquad (3.1)$$

where S_j is the jth triangle grid area and it is ensured positive by counting the vertices in the contour-clockwise order. $\underline{S}$ is the lower bound of the triangle grid area which is a small positive number to prevent the intersection. m is the number of triangle grids involved.

Inspired by this non-intersection constraint, the triangle grid areas are also constrained with an upper bound in this work, in order to realize the local geometry control. It is:

$$S_j \leq \bar{S} \quad j = 1, \dots, m \qquad (3.2)$$

in which $\bar{S}$ is the upper bound of the triangle grid area. $\bar{S}$ is determined by the specific problem applied. For instance, if the method is applied to designing wire-wrapped screens for sand protection, then $\bar{S}$ is determined by the minimum sand size to be blocked; if the method is applied to designing lattice structures for permeability control, then $\bar{S}$ is determined by the maximum local permeability allowed.

3.2. The local grid incircle radius

Another method of realizing local geometry control is to constrain the incircle radius (see Fig. 2), with which the maximum incircle radius constraint can be applied as:

$$R_j \leq \bar{R} \quad j = 1, \ldots, m$$
$$R_j = \frac{2S_j}{P_j} \tag{3.3}$$

where P_j is the perimeter of the jth triangle grid.
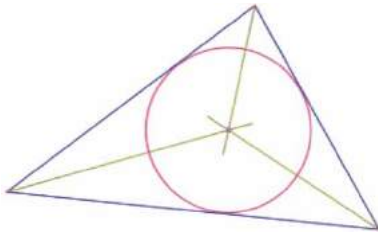

Figure 2. In-circle of the triangle grid.

As well, the minimum incircle radius constraint should be simultaneously applied to preventing the edge flipping, which is:

$$R_j \geq \underline{R} \quad j = 1, \ldots, m \tag{3.4}$$

The purpose of controlling the incircle radius is that, the aspect ratio can be kept small which means close-to-isotropic properties.

4. Case study

A few numerical examples will be studied in this subsection to prove the effectiveness of the local geometry control.

4.1. Shape optimization examples

In Fig. 3, the initial truss structure and the attached boundary conditions are demonstrated. Two point forces are loaded with the magnitude of 0.1/each. All truss elements employ the section area of 0.04 and the material Young's modulus of 1.3.
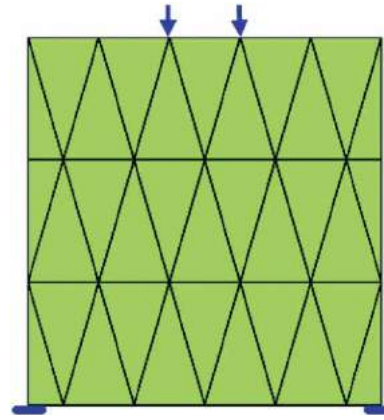

Figure 3. The initial truss structure (overall size of 5*5.19) and the boundary conditions.

A few shape optimization processes are gone through with different $\bar{S}$ values and the fixed $\underline{S} = 0.3$. Correspondingly, the optimization results are demonstrated in Fig. 4. The derived structural compliance values are attached in the figure caption.

Some interesting conclusions can be drawn from the optimization results that:

- The shape optimization result without local grid area constraint is only a local optimum, and a similar conclusion can be found in [18];
- In case that the grid area constraints are applied, the derived structural compliance value is non-monotonically varying against the $\bar{S}$ value;
- Restricting the maximum grid area can possibly help converge the result at a better local optimum; see Fig 4(f–h).

Then, more shape optimization processes are performed with different $\bar{R}$ values and the fixed $\underline{R} = 0.1$. The optimization results are shown in Fig. 5 and the derived structural compliance values are attached in the figure caption.

Conclusions of this example is different as compared to the last one, which is:

- In case that the grid incircle radius is constrained, the derived structural compliance value is monotonically varying against the $\bar{R}$ value. A smaller $\bar{R}$ value would lead to a less optimal design solution;
- The non-constrained design solution shows the best structural performance.

4.2. Topology optimization example

In the shape optimization examples, the truss element densities keep unchanged, and therefore, no topological change happens. For the following example, the
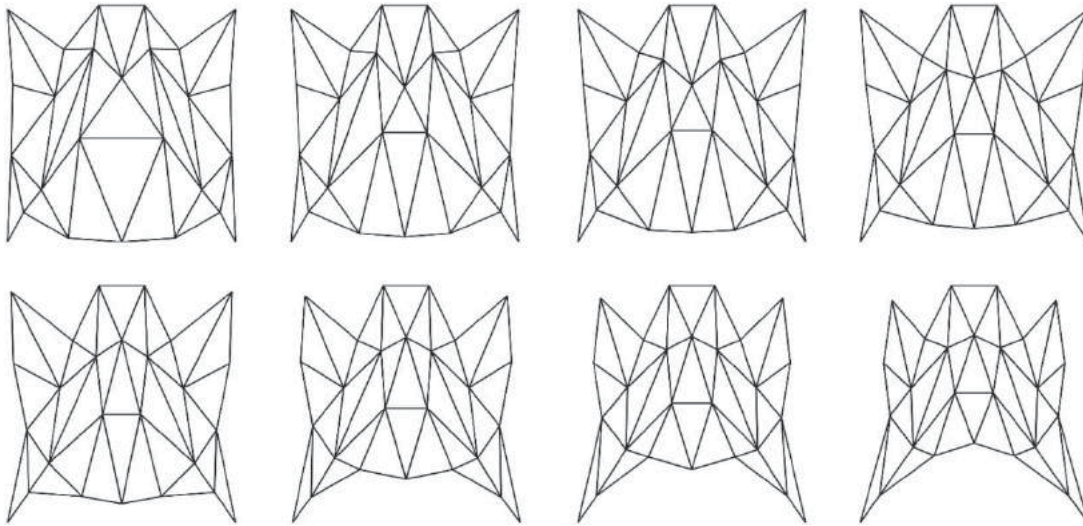
Figure 4. Shape optimization results with different $\bar{S}$ values: (a) $\bar{S} = +\infty; obj = 0.9136$, (b) $\bar{S} = 1.15; obj = 0.9354$, (c) $\bar{S} = 1.05; obj = 0.9503$, (d) $\bar{S} = 0.95; obj = 0.9729$, (e) $\bar{S} = 0.85; obj = 0.9580$, (f) $\bar{S} = 0.75; obj = 0.9102$, (g) $\bar{S} = 0.65; obj = 0.9062$, and (h) $\bar{S} = 0.55; obj = 0.8949$.
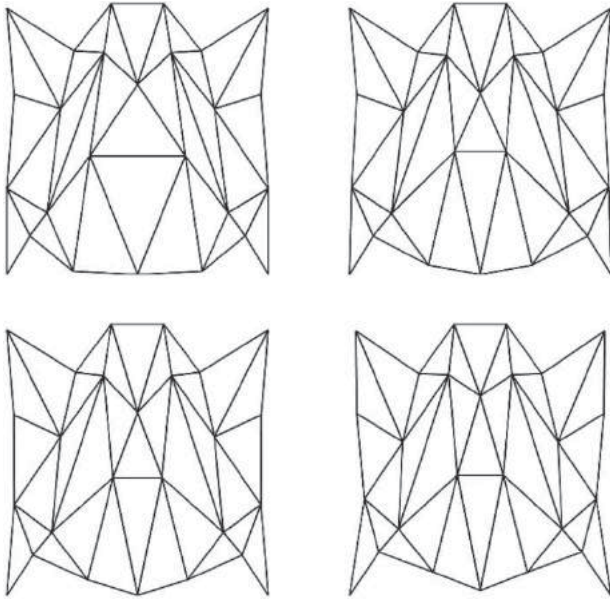

Figure 5. Shape optimization results with different $\bar{R}$ values: (a) $\bar{R} = +\infty; obj = 0.9099$, (b) $\bar{R} = 0.40; obj = 0.9315$, (c) $\bar{R} = 0.38; obj = 0.9451$, (d) $\bar{R} = 0.36; obj = 0.9617$.

same input ground structure and boundary conditions as demonstrated in Fig. 3 are applied. Both nodal positions and truss element densities are employed as design variables. Hence, both shape and topological changes could happen. As discussed in Section 1, the simultaneous optimization approach is employed and it is intended to remove 8 truss elements from the input ground structure.

For the local geometry control, it would be more complex compared to the shape optimization examples. If a truss element density approaches to zero, the two connected triangle grids will merge into a quadrangle

grid. At the same time, the local constraints will dynamically change as well which causes the non-smooth convergence. This phenomenon should be taken care specially, and based on the numerical examples studied; the overall convergence is not severally influenced.

A few topology optimization processes are gone through with different $\bar{S}$ values and fixed at $\underline{S} = 0.3$. Correspondingly, the optimization results are demonstrated in Fig. 6.

By analyzing the design solutions in Fig. 6, the following conclusion can be derived:

- In case that the grid area is constrained, the derived structural compliance value is monotonically varying against the $\bar{S}$ value.
- A smaller $\bar{S}$ value would lead to a less optimal design solution;
- The non-constrained design solution shows the best structural performance.
- Topology of the non-constrained design solution is different from those of the constrained design solutions.
- Because of the removed struts, the structural performances of the topology optimization results are not so good as compared to those of the shape optimization results.

The convergence history of a topology optimization process is recorded in Fig. 7. We can see that fluctuations happen during the early iterations when some grids merge and the locally constrained objects dynamically change. Then, in the later iterations, the topology is no longer varying while the nodal positions are optimized to smoothly converge to the final optimum.
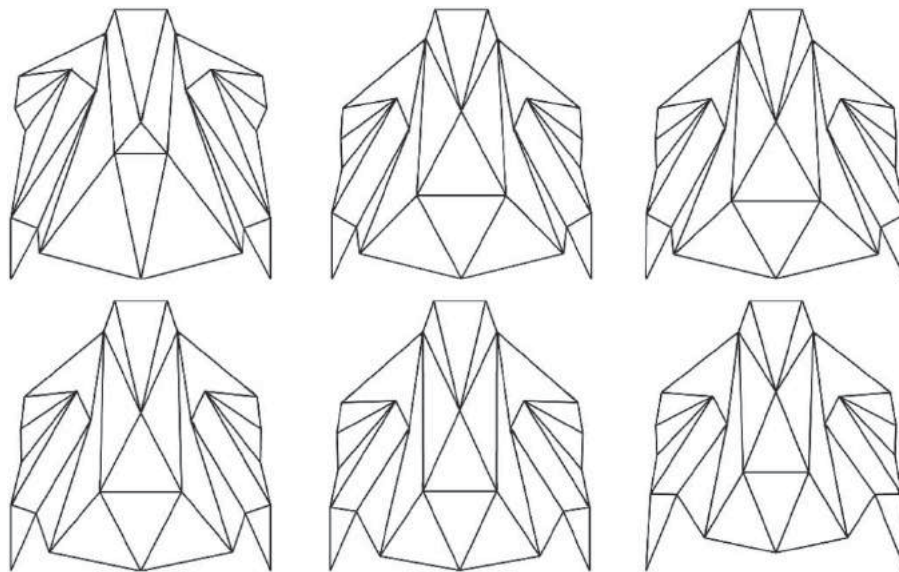
Figure 6. Shape optimization results with different $\bar{S}$ values: (a) $\bar{S} = +\infty$; $obj = 1.0129$, (b) $\bar{S} = 1.4$; $obj = 1.1218$, (c) $\bar{S} = 1.3$; $obj = 1.1335$, (d) $\bar{S} = 1.2$; $obj = 1.1531$, (e) $\bar{S} = 1.1$; $obj = 1.1711$, and (f) $\bar{S} = 1.0$; $obj = 1.2019$.
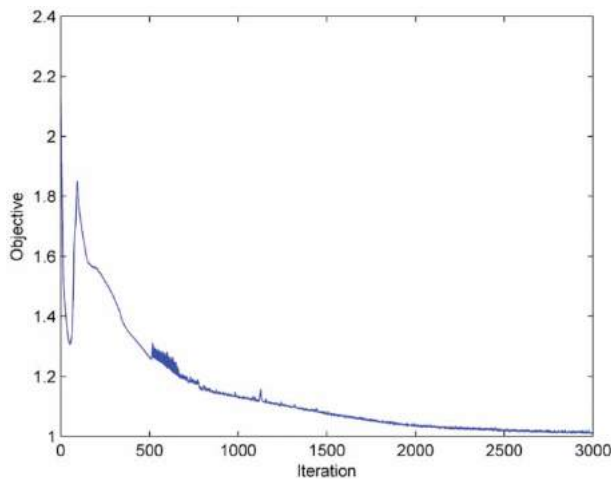

Figure 7. Convergence history of a topology optimization process.

Figure 9. The optimization result.

4.3. A benchmark study

In this sub-section, a benchmark example is studied with local grid area control, which was previously studied in [18]. In Fig. 8, the left ha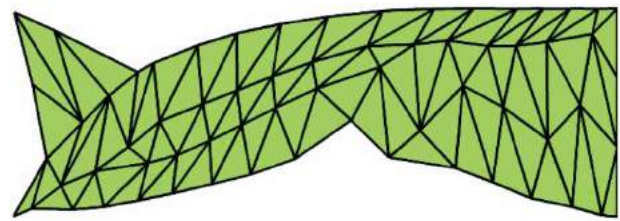lf of the initial truss structure is demonstrated and the red line represents the symmetry axis. The bottom feet are fixed and one point force is loaded on the top midpoint with the magnitude of 0.1. All truss elements employ the section area of 0.04 and the material Young's modulus of 1.3. For the local grid area constraint, $\bar{S}$ equals 1.0 and $\underline{S}$ is 0.3.

The optimization result is demonstrated in Fig. 9. We can conclude from this result that, the load path has been effectively optimized by changing the nodal positions; more importantly, the local grid area is strictly constrained below 1.0, which is not achieved in the previous work [18].
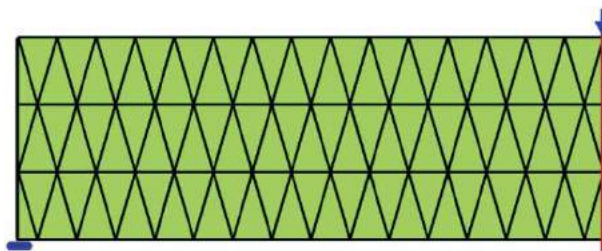

Figure 8. The initial truss structure (overall size of 30*5.19) and the boundary conditions.

5. Conclusion

This paper presents a truss-like structure design method with constrained local geometry. Two local geometry measures are proposed: the local grid area and the local grid incircle radius. Both measures have been proven effective in constraining the local geometry.

Through the numerical examples, it has been observed that the upper bound of the local geometry constraint has an influence in the result optimality: either positive or negative depending on the specific problems. A discussion has been provided to explain this phenomenon; however, more exploration will be made in our future work to dig the deep reasons.

On the other hand, the proposed method will be extended to 3D examples in the future work to better serve the practical engineering design tasks.

Acknowledgement

ORCID

Jikai Liu http://orcid.org/0000-0002-9732-3791
Yongsheng Ma http://orcid.org/0000-0002-6155-0167

References

[1] Achtziger, W.: On simultaneous optimization of truss geometry and topology, Structural and Multidisciplinary Optimization, 33(4), 2007, 285–304. http://dx.doi.org/10.1007/s00158-006-0092-0
[2] Alzahrani, M.; Choi, S. K.; Rosen D. W.: Design of truss-like cellular structures using relative density mapping method, Materials and Design, 85, 2015, 349–360. http://dx.doi.org/10.1016/j.matdes.2015.06.180
[3] Asadpoure, A.; Guest, J. K.; Valdevit, L.: Incorporating fabrication cost into topology optimization of discrete structures and lattices, Structural and Multidisciplinary Optimization, 51(2), 2015, 385–396. http://dx.doi.org/10.1007/s00158-014-1133-8
[4] Bendsoe, M. P.; Ben-Tal, A.; Zowe, J.: Optimization methods for truss geometry and topology design, Structural Optimization, 7(3), 1994, 141–159. http://dx.doi.org/10.1007/BF01742459
[5] Bendsoe, M. P.: Optimization of structural topology, shape, and material, Springer, Berlin Heidelberg, 1995
[6] Bendsoe, M. P.; Sigmund, O.: Topology optimization – theory, methods and applications, 2nd edition, Springer, Berlin Heidelberg, 2003.
[7] Ben-Tal, A.; Bendsoe, M. P.: A new method for optimal truss topology design, SIAM Journal on Optimization, 3(2), 1993, 322–358. http://dx.doi.org/10.1137/0803015

[8] Cui, C. Y.; Jiang, B. S.: A morphogenesis method for shape optimization of framed structures subject to spatial constraints, Engineering Structures, 77, 2014, 109–118. http://dx.doi.org/10.1016/j.engstruct.2014.07.032
[9] Dorn, W. S.; Gomory, R. E.; Greenberg, H. J.: Automatic design of optimal structures, Journal de Mecanique, 3(1), 1964, 25–52.
[10] Hagishita, T.; Ohsaki, M.: Topology optimization of trusses by growing ground structure method. Structural and Multidisciplinary Optimization, 37(4), 2009, 377–393. http://dx.doi.org/10.1007/s00158-008-0237-4
[11] Kocvara, M.; Zowe, J.: How to optimize mechanical structures simultaneously with respect to geometry and topology, In: Olhoff N, Rozvany GIN (eds) First world congress of structural and multidisciplinary optimization, Pergamon, Oxford, 1995.
[12] Liu, J. K.; Ma, Y. S.; Fu, J. Y.; Duke, K.: A novel CACD/CAD/CAE integrated design framework for fiber-reinforced plastic parts, Advances in Engineering Software, 87, 2015, 13–29. http://dx.doi.org/10.1016/j.advengsoft.2015.04.013
[13] Martinez, P.; Marti, P.; Querin, O. M.: Growth method for size, topology, and geometry optimization of truss structures, Structural and Multidisciplinary Optimization 33(1), 2007, 13–26. http://dx.doi.org/10.1007/s00158-006-0043-9
[14] McKeown, J. J.: Growing optimal pin-jointed frames, Structural Optimization, 15(2), 1998, 92–100. http://dx.doi.org/10.1007/BF01278495
[15] Stegmann, J.; Lund, E.: Discrete material optimization of general composite shell structures, International Journal for Numerical Methods in Engineering, 62(14), 2005, 2009–2027. http://dx.doi.org/10.1002/nme.1259
[16] Tang, Y. L.; Kurtz, A.; Zhao, Y. F.: Bidirectional Evolutionary Structural Optimization (BESO) based design method for lattice structure to be fabricated by additive manufacturing, 69, 2015, 91–101. http://dx.doi.org/10.1016/j.cad.2015.06.001
[17] Wang, D.; Zhang, W. H.; Jiang, J. S.: Combined shape and sizing optimization of truss structures, Computational Mechanics, 29(4), 2002, 307–312. http://dx.doi.org/10.1007/s00466-002-0343-x
[18] Xia, Q.; Wang, M. Y.; Shi, T. L.: A method for shape and topology optimization of truss-like structure, Structural and Multidisciplinary Optimization, 47(5), 2013, 687–697. http://dx.doi.org/10.1007/s00158-012-0844-y
[19] Yan, J.; Cheng, G. D.; Liu, S. T.; Liu, L: Comparison of prediction on effective elastic property and shape optimization of truss material with periodic microstructure. International Journal of Mechanical Science, 48(4), 2006, 400–413. http://dx.doi.org/10.1016/j.ijmecsci.2005.11.003
[20] Zhang, W. H.; Sun, S. P.: Scale-related topology optimization of cellular materials and structures, International Journal for numerical methods in Engineering, 68(9), 2006, 993–1011. http://dx.doi.org/10.1002/nme.1743
[21] Zegard, T.; Paulino, G. H.: GRAND – Ground structure based topology optimization for arbitrary 2D domains using MATLAB, Structural and Multidisciplinary Optimization, 50(5), 2014, 861–882. http://dx.doi.org/10.1007/s00158-014-1085-z